Thin Solid Films 605 (2016) 64–72

Contents lists available at ScienceDirect

Thin Solid Films

journal homepage: www.elsevier.com/locate/tsf

Effect of hydrogen doping on the properties of Al and F co-doped ZnO films for thin film silicon solar cell applications

Fang-Hsing Wang *, Tung-Hsin Yang

Department of Electrical Engineering and Graduate Institute of Optoelectronic Engineering, National Chung Hsing University, No. 250, Kuo-Kuang Rd., Taichung 40227, Taiwan, ROC

A R T I C L E I N F O

Article history:
Received 7 May 2015
Received in revised form 2 October 2015
Accepted 2 October 2015
Available online 14 October 2015

Keywords:
Transparent conducting oxide
Aluminum and fluorine co-doped zinc oxide
Thin films
Hydrogen
Magnetron sputtering

A B S T R A C T

Aluminum and fluorine co-doped zinc oxide (AFZO) thin films were prepared in Ar + H_2 atmospheres by rf magnetron sputtering at room temperature. The structural, electrical, and optical properties of the prepared films were investigated using X-ray diffraction, scanning electron microscopy, atomic force microscopy, Hall-effect measurement, X-ray photoelectron spectroscopy, and ultraviolet–visible spectrometry, and their dependence on deposition atmosphere (i.e. H_2 / (H_2 + Ar) ratio) was studied. The resulting films showed a (0 0 2) diffraction peak, indicating a typical wurtzite structure, and the optimal film crystallinity was obtained with the H_2 / (H_2 + Ar) ratio of 3%. The electrical resistivity of AFZO films decreased to 9.16×10^{-4} Ω-cm, which was lower than ZnO:Al and ZnO:F films due to double doping effect of Al and F. The resistivity further decreased to below 5×10^{-4} Ω-cm for the AFZO film with the H_2 / (H_2 + Ar) ratio of 3%–5%. All the films regardless of hydrogen content displayed high transmittances (>92%) in the visible wavelength range. Applying the developed AFZO films as front transparent electrodes, amorphous Si thin film solar cells were fabricated and the open-circuit voltage, fill factor, and efficiency of the cell with the hydrogenated AFZO film were improved in contrast to those without the hydrogenated film.

© 2015 Elsevier B.V. All rights reserved.

1. Introduction

Transparent conducting oxide films are indispensable materials in optoelectronic industry for application such as solar cells, flat panel displays, light-emitting diodes, electrochromic windows and low thermal emissivity windows [1–5]. Impurity-doped ZnO thin films have attracted considerable attention as transparent conducting oxide (TCO) thin films due to their superior electrical and optical properties in combination with the low material cost and non-toxicity as compared to tin-doped indium oxide (ITO) films [6–10]. Moreover, high electrical and optical stability under hydrogen plasma promoted ZnO thin films as front electrodes in silicon thin film solar cells.

Many cationic dopants such as boron [6], aluminum [7,8], gallium [9,10], indium and titanium [11] have been studied to substitute for Zn to improve the conductivity of n-type ZnO films. Among these dopants, Al-doped ZnO (AZO) thin films have been widely studied as a substitute for ITO films due to low cost and superior stability under hydrogen plasma [12]. Our previous study shows that the resistivity of the sputtered AZO thin film is below 2×10^{-3} Ω-cm, which is remarkably lower than undoped ZnO films with a typical resistivity of 1–100 Ω-cm [13]. Besides, fluorine has attracted attention because it can substitute for oxygen as an anionic dopant in the ZnO atomic structure to provide an extra conducting electron. The ionic radius of fluorine (0.131 nm) is close to that of oxygen (0.138 nm), thus resulting in less lattice distortion in ZnO crystal structure [14,15]. Gordon et al. reported that the substitution of oxygen ions by fluorine ions would perturb the valence band, thereby leaving the conduction band relatively free from scattering, which could enhance carrier mobility and reduce light absorption [16]. Furthermore, there has been particular interest in the role of hydrogen in ZnO because density function theory and total energy calculations suggest that hydrogen should be a shallow donor for improvement of conductivity of ZnO-based films [17–19].

Several methods such as sol–gel [20–22], spray deposition [23], and magnetron sputtering [24–26] had been proposed to prepare the Al and F co-doped ZnO (AFZO) thin films. Among these methods, magnetron sputtering is the most commonly used technique due to high deposition rate at low temperature, high film uniformity, and large area films with strong adhesion. Kim et al. prepared AFZO films by magnetron sputtering of a ZnO:Al_2O_3 target at substrate temperature of 150 °C with Ar/CF_4/H_2 gas mixtures, and annealed in vacuum at 300 °C [24]. They reported that the lowest resistivity of the as-deposited/vacuum-annealed films was about 3.9–4×10^{-4}/2.9×10^{-4} Ω-cm. Kim et al. used two ceramic targets, i.e. ZnO:Al_2O_3 (3 wt%) and ZnO:ZnF_2 (0–10 wt%), to co-sputter AFZO films with varying fluorine contents to investigate doping effects of fluorine on properties of the films [25]. Their results indicated that the small amount of F addition to AZO films resulted in an improved electrical conductivity by enhancing Hall mobility, and the minimum resistivity was as low as 5.9×10^{-4} Ω-cm.

* Corresponding author.
E-mail address: fansen@dragon.nchu.edu.tw (F.-H. Wang).

http://dx.doi.org/10.1016/j.tsf.2015.10.020
0040-6090/© 2015 Elsevier B.V. All rights reserved.

In this paper, we use a single ceramic ZnO target containing Al_2O_3 (1 wt%) and ZnF_2 (1.5 wt%) to fabricate hydrogenated AFZO thin films by rf-magnetron sputtering in Ar + H_2 atmospheres at room temperature. The structural, optical, and electrical properties of hydrogenated AFZO thin films are investigated with various H_2 flow rates. The superstrate p-i-n amorphous Si (α-Si) thin film solar cells using the AFZO thin films as the front transparent electrodes are developed and their current–voltage characteristics are measured.

2. Experimental details

The ZnO powder (99.999%), Al_2O_3 powder (99.999%) and ZnF_2 powder (99.995%) were mixed with the ratio of 97.5 wt%, 1.0 wt%, and 1.5 wt%, respectively, and then ball milled for 24 h in alcohol. After being dried and ground, the powders were uniaxially pressed into pellets of 3 mm thickness and 52 mm diameter. The pressed targets were sintered at 1060 °C for 3 h to prepare the ceramic target for sputtering. Glass substrates (Corning Eagle XG) were cleaned ultrasonically with isopropyl alcohol (IPA) and deionized (DI) water, and then dried under a blown nitrogen gas. AFZO films of approximately 330 nm were deposited on glass substrates by using an rf-magnetron sputtering system at an rf power of 80 W at room temperature. The working distance from the target to substrates is 8 cm. Ar or Ar + H_2 were introduced into the chamber and the working pressure was controlled at 0.667 Pa (5 mTorr) with the different H_2 / (H_2 + Ar) ratios of 0–10%. During sputtering, the substrate holder was spun at 10 rpm for a better film uniformity.

The structure of the films was analyzed by X-ray diffraction (XRD) (PANalytical) with Cu-Kα radiation ($\lambda = 1.54056$ Å, θ–2θ scan mode). The electrical resistivity, Hall mobility, and carrier concentration were determined by Hall-effect measurement (Ecopia, HMS-300) using the Van der Pauw method. The morphology of AFZO films was observed using a field emission scanning electron microscope (FE-SEM) (JEOL, JSM-6700F) and an atomic force microscope (AFM) (Veeco, D3100). The optical transmittance was obtained by a UV–visible spectrophotometer (JASCO, V–570). X-ray photoelectron spectroscopy (XPS) (ULVAC-PHI, PHI 5000 Versaprobe) characterization was made after surface pre-cleaning for 30 s. The pre-cleaning of the samples used Ar^+ ion sputtering with an operation voltage of 2 kV and a sputtering rate of 12.5 nm/min in SiO_2. Wide-scan spectra in the 0–1100 eV kinetic energy range were recorded in 1 eV steps. Detailed spectra of the core level lines were recorded in 0.2 eV steps.

Thin film solar cells were fabricated using a single-chamber plasma enhanced chemical vapor deposition system at 200 °C with an rf power of 20 W and a working pressure of 93.31 Pa (0.7 Torr) on a 0.2%-HCl etched AFZO thin films with a thickness of about 800 nm. The thicknesses of the p/i/n α-Si layers are about 20/400/50 nm. The detailed fabrication processes have been reported previously [27]. The current–voltage characteristics of the fabricated solar cells were measured under an illumination intensity of 300 mW/cm^2 and an air mass (AM) 1.5G spectrum.

3. Results and discussion

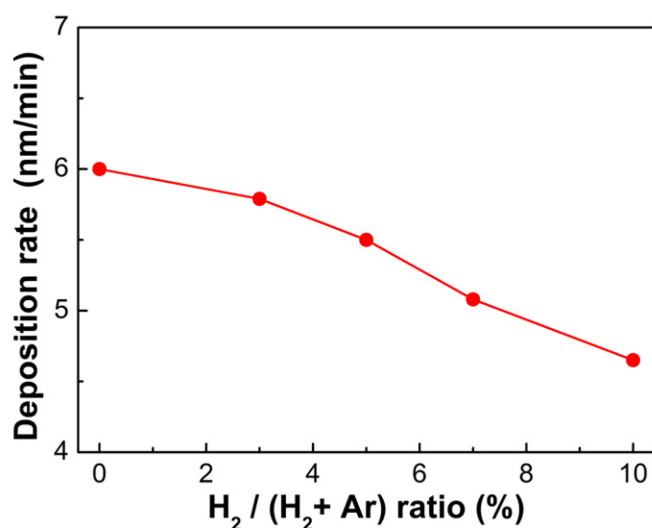

Fig. 1. Deposition rate of AFZO:H thin films as a function of H_2/(H_2 + Ar) ratio.

Fig. 1 shows the deposition rates of AFZO:H thin films as a function of H_2/(Ar + H_2) ratio. The decreased deposition rate with the increasing H_2 ratio is due to the gas dilution effect and possible chemical reaction of hydrogen with oxygen in the plasma ambient. Fig. 2 exhibits the XRD patterns of AFZO:H thin films with various H_2/(Ar + H_2) ratios. All the AFZO:H films showed a (0 0 2) diffraction peak, indicating a typical wurtzite structure with a preferential orientation of the c-axis perpendicular to the substrate. No Al_2O_3 and ZnF_2 phase existed in the XRD patterns. With increasing the H_2/(Ar + H_2) ratio, the intensity of the (0 0 2) peak increased first and then decreased as the hydrogen ratio was larger than 3%, indicating the AFZO films incorporated with small amount hydrogen possessed better crystallinity. This phenomenon results from excess hydrogen may adsorbed on the growing surface, restraining further crystal growth with preferred orientation and leading to poor crystallinity of the films [28]. Liu et al. also reported that the H_2 flow rate should be controlled in a small range to grow good crystallinity AZO thin films [29]. Table 1 lists the structural parameters of AFZO films calculated from the XRD results (as shown in Fig. 2). The grain sizes of the AFZO films with different H_2/(Ar + H_2) ratios are evaluated from the full-width at half-maximum (FWHM) of the (0 0 2) peak using Scherrer's formula [30]. The crystalline plane distance, d, is calculated from the Bragg diffraction equation: $\lambda = 2d\sin\theta$, where λ is the X-ray wavelength (1.54056 Å) and θ is the diffraction angle of the (0 0 2) peak. The lattice constant, c, is equal to 2d for the (0 0 2) diffraction peak. The residual film strain (ε) can be estimated by the relative changes of the lattice constant and is associated with the diffraction peak displacement, that is, $\varepsilon = [(c_{film} - c_{bulk}) / c_{bulk}]$, where c_{bulk} is the unstrained lattice parameter measured from bulk ZnO [31]. In the AFZO films, Al (or F) is expected to substitute Zn (or O) in its lattice site, thus shifting the (0 0 2) peak position to higher 2θ values, owing to the smaller ionic radius of Al^{3+} (or F^-) than Zn^{2+} (or O^{2-}) [14,32]. In this work, the (0 0 2) peak position of the AFZO films is situated at $2\theta = 34.41°$, which almost consists with hexagonal ZnO of 34.42° with the wurtzite structure (JCPDS 36-1451) [33] and is smaller than that of AZO films (around 34.5°) [29,32]. This fact implies that many F atoms maybe situate in interstitial sites rather than substitute for O^{2-} ions. In the AFZO:H films, the (0 0 2) peak shifted toward lower

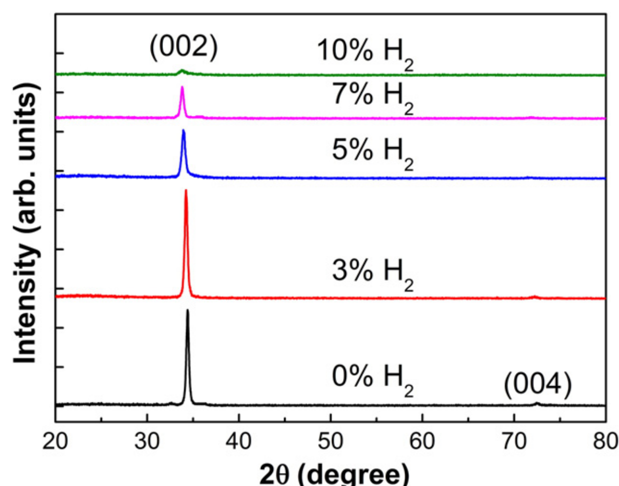

Fig. 2. XRD pattern and of AFZO:H thin films prepared with different H_2/(H_2 + Ar) ratios.

Table 1
Structural parameters of AFZO thin films calculated from the XRD patterns.

$H_2/(H_2 + Ar)$ ratio (%)	(002) peak 2θ (°)	FWHM (°)	Grain size (nm)	d (nm)	c (nm)	Strain ($\times 10^{-3}$)
0	34.41	0.319	26.0	0.2604	0.5208	0.262
3	34.24	0.344	24.1	0.2617	0.5233	5.08
5	34.14	0.404	20.6	0.2624	0.5248	7.93
7	33.94	0.459	18.1	0.2639	0.5278	13.7
10	33.76	0.710	11.7	0.2653	0.5306	18.9

diffraction angle (from 34.41° to 33.76°), leading to an increased crystalline plane distance and a large compressive strain in the films. This shift in the 2θ angle can attribute to hydrogen atoms occupying the Zn–O bond center, as indicated by the smaller diffraction angle for the sample deposited with H_2 doping [34]. The estimated grain size decreased from 26.6 to 16.9 nm with increasing the $H_2/(Ar + H_2)$ ratio from 0 to 10%. Liu et al. reported that the crystallinity of the AZO:H film was improved and the grain size became larger when the hydrogen atoms situated in the Zn–O bond center was at saturation stage [29]. However, Addonizio et al. found that the grain size of AZO:H films decreased with the hydrogen ratio increased from 1% to 40% [35]. In this work, the observed trend of the grain size agrees with the result of Addonizio et al.

Fig. 3 displays the plane-view and cross-section view FE-SEM images of AFZO thin films with the $H_2/(Ar + H_2)$ ratios of 0%, 5%, and 10% at an accelerating voltage of 3.0 kV. The AFZO films with the lower hydrogen content exhibited more dense morphology and larger surface grain size. All films showed a columnar structure. Lee reported that when AZO film was deposited with high hydrogen ratio (i.e., 25%), columnar grains disappeared [36]; however, in this work the AFZO film with the $H_2/(Ar + H_2)$ ratios of 10% still exhibited a clear columnar structure. The observations from SEM images consist with the XRD data.

Fig. 4 exhibits the AFM images of AFZO thin films with the $H_2/(Ar + H_2)$ ratios of 0%, 5%, and 10%. The images are obtained in tapping mode taken over a scale of $5 \times 5\ \mu m^2$. The root mean square (RMS) roughness of the surface monotonically increased from 3.07 nm to 9.76 nm as the $H_2/(Ar \pm H_2)$ ratio increased from 0% to 10%. The earlier literatures have investigated the influence of hydrogen doping on surface morphology of doped ZnO films: the surface roughness of AZO, ZnO, and ZnO:Ti films increases with the hydrogen partial pressure or hydrogen flow rate in sputtering ambient [11,36,37]; while ZnO:In films exhibits a different phenomenon: its surface roughness significantly decreases with the incorporation of hydrogen [38].

Fig. 5 shows the resistivity, carrier concentration, and Hall mobility of AFZO thin films deposited at various $H_2/(Ar + H_2)$ ratios. Results of FZO:H thin films were also shown in the figure for comparison. The resistivity of the unhydrogenated AFZO thin film was $9.16 \times 10^{-4}\ \Omega$-cm, which was lower than $3.08 \times 10^{-3}\ \Omega$-cm of FZO films and $1.74 \times 10^{-3}\ \Omega$-cm of AZO films. The significant decrease of resistivity was caused by the increase of carrier concentration as well as Hall mobility. This fact demonstrates that double doping of Al and F is more effective than either Al or F doping for improving conductivity of ZnO films. In AFZO:H films, the resistivity decreased first with increasing $H_2/(Ar + H_2)$ ratio and reached a minimum ($4.41 \times 10^{-4}\ \Omega$-cm) at the ratio of 3%, which was attributed to the increase in both carrier concentration and Hall mobility by small amount hydrogen doping. With further increasing hydrogen content, the carrier concentration reached a maximum at the ratio of 5–7% and Hall mobility monotonically decreased. It has been shown that O–H (in H^+ form) stretch in Zn–O bond has the lowest formation energy, and the doped hydrogen acts as an n-type donor in ZnO related films [19,39]. Also, hydrogen can be incorporated into ZnO related films as an interstitial, and form dangling bonds at the grain boundaries [19]. The increase in carrier concentration upon addition of hydrogen is thought to stem from the formation of O–H stretch inside Zn–O bonds. The decrease in the Hall mobility with the increasing $H_2/(Ar + H_2)$ ratio may result from both ionized impurity scattering and grain boundary scattering due to more hydrogen and smaller grain size in the films [40]. The beneficial effect of hydrogen doping was also found in FZO films. Although the carrier concentration and the Hall mobility of the FZO films were lower than those of the AFZO films at the low $H_2/(Ar + H_2)$ ratios of 0–5%, however, the results were reversed at the high $H_2/(Ar + H_2)$ ratios of 7–10%. The reason may be due to that the rapid increase of doping impurities in AFZO:H films reaches a saturation stage and then excess impurities situate in interstitial sites and grain boundaries, leading to carrier scattering and thus increasing resistivity [24].

The XPS study was performed to investigate the chemical states of elements in the AFZO films for clarifying mechanisms of the improvement in resistivity. Fig. 6 shows the XPS full spectra of AFZO thin films

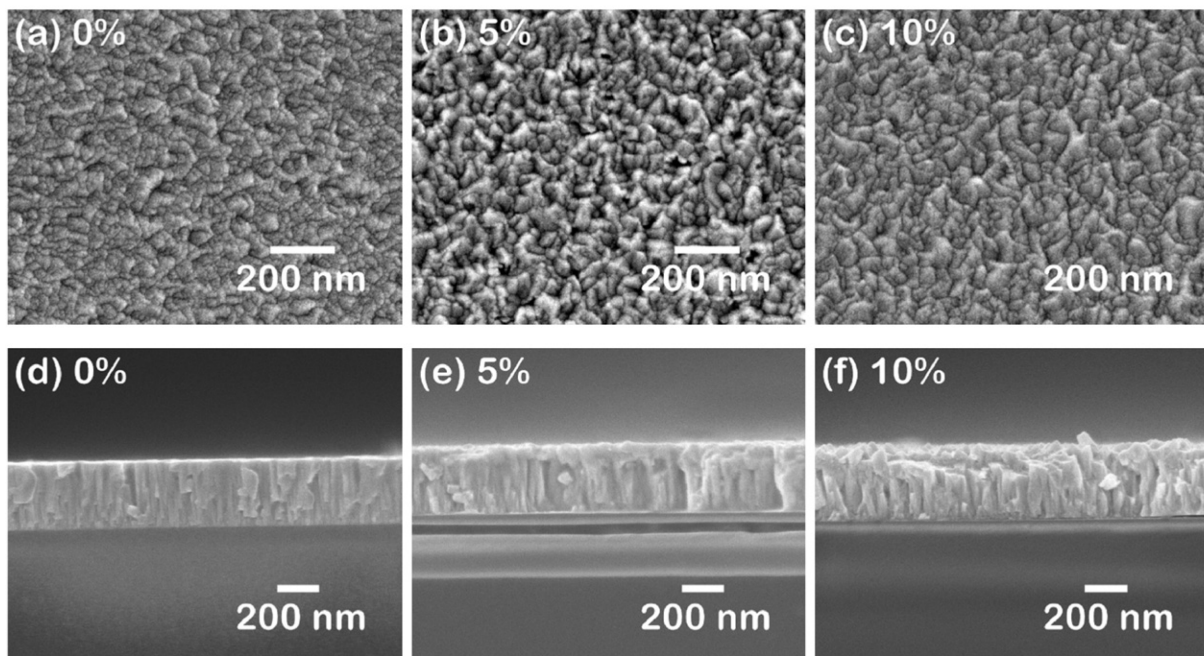

Fig. 3. FE-SEM images of AFZO:H thin films: plane-view (a) 0%, (b) 5%, and (c) 10%; cross-section view (d) 0%, (e) 5%, and (f) 10%.

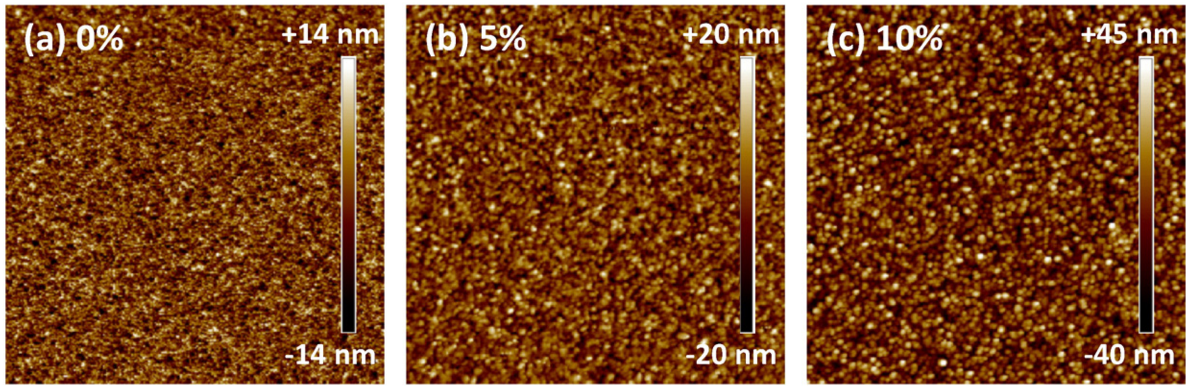

Fig. 4. AFM images of AFZO:H thin films with the $H_2/(H_2 + Ar)$ ratios: (a) 0%, (b) 5%, and (c) 10%.

with different $H_2/(Ar + H_2)$ ratios. Zn, O, Al, and C peaks were detected as shown in the spectra. The Al peak was not obvious in the wide-scan spectra with low number of data points per electron-volt due to the low content and the low values of the ionization cross sections of Al [41], while it appeared in the narrow-scan spectra as shown in Fig. 7. The F peak was not observed due to very few detectable fluorine (<0.1%) in the films. The C 1s line at 284.6 eV was used to calibrate the binding energy scale for XPS measurements. Table 2 lists relative surface concentration ratios of the elements in AFZO:H thin films. The detected carbon is related to the carbon contamination in the sputtering chamber and carbon adsorbed on the surface during the exposure of the film to the ambient atmosphere. Fig. 7 shows the details of O 1s, Al 2p, and Zn 2p core line deconvolution for the AFZO films with the $H_2/(Ar + H_2)$ ratio of 0% and 5%. The XPS peak decomposition and peak area were determined using XPSPEAK version 4.1 software with a symmetric Gaussian–Lorentzian function and linear backgrounds. The peak position was constrained, and the FWHM of the synthetic peaks was fixed from the spectrum of one species to the other. The area of the synthetic peak was allowed to vary in the peak fitting process. In Fig. 7(a) and (b), the bonding states of O 1s spectra are resolved into three components centered at 530.1 ± 0.1 (O_I), 531.2 ± 0.2 (O_{II}) and 532.4 ± 0.2 eV (O_{III}), respectively [42]. The O_I component is attributed to O_2^- ions on the wurtzite structure of the hexagonal Zn^{2+} ion array. That is, the O_I component can be attributed to Zn–O bonds. The O_{II} component is associated with O_2^- ions in oxygen-deficient regions within the ZnO matrix. The O_{III} component is usually attributed to chemisorbed or dissociated oxygen or OH species on the film surface [8,42]. For the AFZO:H (5%) films, the area ratio of O_I component decreased and O_{II} component increased, indicating an increase in oxygen vacancies. This result contributes to the increase of the carrier concentration in the hydrogenated AFZO films. Fig. 7(c) and (d) shows the four resolved components of the Al $2p_{3/2}$ for the AFZO films with the $H_2/(Ar + H_2)$ ratio of 0% and 5%, respectively. The low binding energy component (Al_I) centered at 72.65 ± 0.1 eV is due to the presence of metallic Al [42]. The Al_{II} and Al_{III} components centered at 73.1 ± 0.1 and 73.75 ± 0.1 eV are attributed to the Al_2O and AlO, respectively [43]. The Al–O bond represents that Al atoms substitute for Zn atoms in AFZO crystals, and therefore can increase the carrier concentration in the films. The Al_{IV} component at 74.7 ± 0.1 eV is due to Al_2O_3

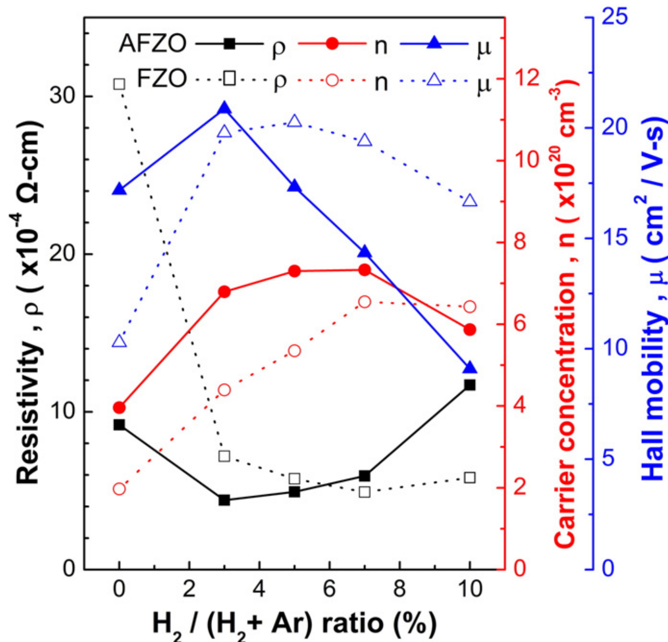

Fig. 5. Electrical properties of AFZO:H thin films as a function of $H_2/(H_2 + Ar)$ ratio.

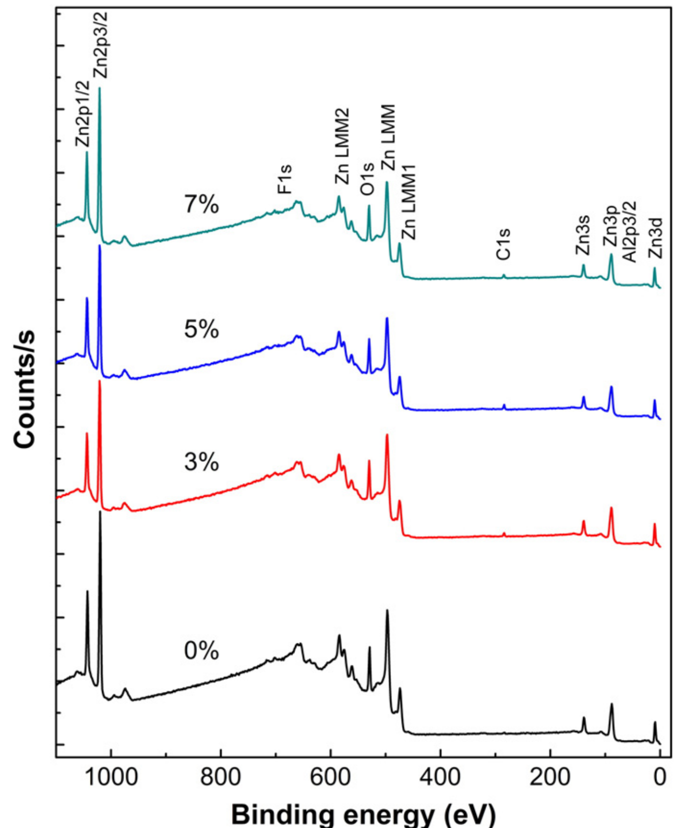

Fig. 6. XPS spectra of AFZO:H thin films with different $H_2/(H_2 + Ar)$ ratios.

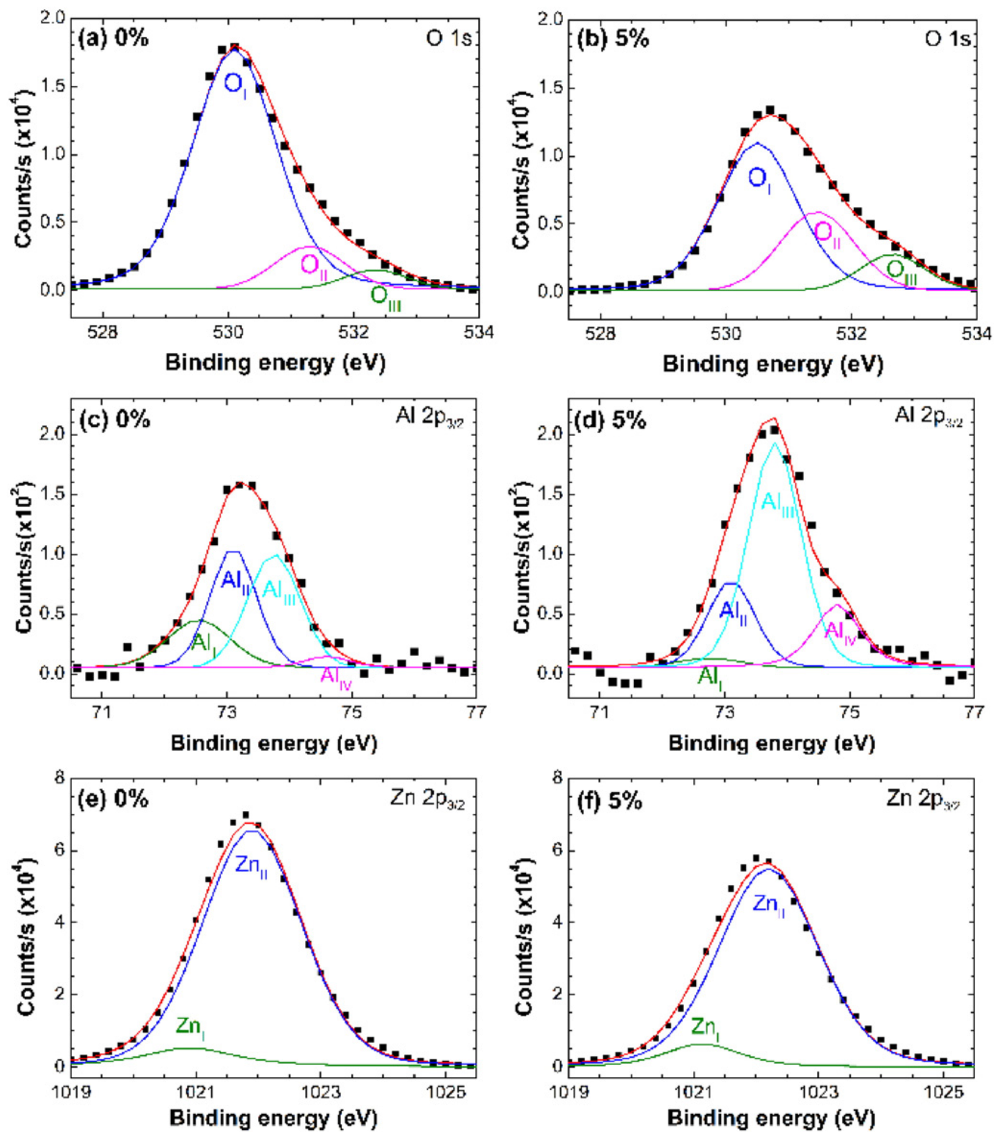

Fig. 7. Details of O 1s, Al 2p, and Zn 2p core line deconvolution for the AFZO films with the $H_2/(H_2 + Ar)$ ratios of 0% and 5%.

formation [44]. For the AFZO:H (5%) films, the apparent increase of the Al_{III} component accompanied the decrease of the Al_I component as compared to the films without hydrogen doping, suggesting that hydrogen incorporated in AFZO films can enhance Al doping effectiveness [45]. Fig. 7(e) and (f) presents the XPS spectra of the Zn $2p_{3/2}$ for the AFZO films with the $H_2/(Ar + H_2)$ ratio of 0% and 5%, respectively. The Zn $2p_{3/2}$ peak is split into two components at 1021.1 $\pm$ 0.2 (Zn_I) and 1022.1 $\pm$ 0.2 eV (Zn_{II}) [8]. The former is due to the presence of metallic Zn, and the latter exhibits the Zn in the oxidized state (Zn–O) [42]. The area ratios of Zn_I and Zn_{II} components almost did not change after incorporation of hydrogen. Moreover, the component peaks slightly shifted toward the higher energy side as compared to the unhydrogenated films, revealing formation of Zn–H bonds in the hydrogenated films [46,47].

Table 2
Relative surface concentration ratios of the elements of AFZO:H films obtained by XPS.

$H_2/(Ar + H_2)$ ratio	0%	3%	5%	7%
Zn 2p	47.8%	45.8%	46.6%	47.4%
O 1s	47.7%	48.7%	47.9%	47.2%
Al 2p	1.2%	1.7%	1.6%	1.7%
F 1s	<0.1%	<0.1%	<0.1%	<0.1%
C 1s	3.20%	3.7%	3.8%	3.6%

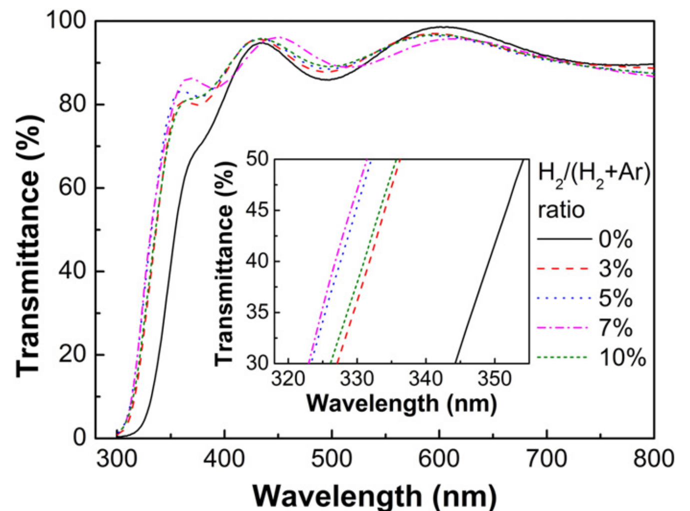

Fig. 8. Optical transmittance of AFZO:H thin films as a function of $H_2/(H_2 + Ar)$ ratio.

Fig. 8 shows the optical transmittance spectra of AFZO thin films deposited under the diverse $H_2/(Ar + H_2)$ ratios. All the films exhibited a very high transmittance larger than 92% when averaged in the visible range from 400 to 700 nm. A marked absorption band edge was found in the vicinity of 350 nm for all the AFZO films due to excitation caused by the absorption of ZnO. No characteristic absorption relating to Al_2O_3 or ZnF_2 was found in the transmission spectra, which agreed with the XRD patterns (as shown in Fig. 2). In addition, the absorption band edge blue-shifted with increasing the $H_2/(Ar + H_2)$ ratio up to 7% and then red-shifted as the $H_2/(Ar + H_2)$ ratio was 10%, as shown in the inset of Fig. 8. The optical properties of ZnO films are related to free carrier absorption and can be expressed by the Drude theory [48]. The dependence of optical absorption coefficient (α) on photon energy ($h\upsilon$) was examined to estimate optical band gap energy (E_g) of the films [49]:

$$\alpha h\upsilon = C(h\upsilon - E_g)^m \tag{1}$$

where m is a constant which determines the type of optical transition ($m = 1/2$ for allowed direct transitions and $m = 2$ for allowed indirect transitions). $(\alpha h\upsilon)^2$ was plotted against the photon energy as shown in Fig. 9. The optical band gaps, which were determined by extrapolating the linear region of the plots to zero absorption, were larger than that of the undoped ZnO (3.37 eV) and increased from 3.68 to 3.88 eV with the increasing $H_2/(Ar + H_2)$ ratio from 0% to 7%. The E_g widening was due to band-filling effect known as the Burstein–Moss shift [50,51]. The band gap widening (ΔE_g) is related to carrier concentration (n_e) in a degenerate semiconductor as the following equation [52]:

$$\Delta E_g = \frac{h^2}{8m^*}\left(\frac{3}{\pi}\right)^{2/3} {n_e}^{2/3}, \tag{2}$$

where h is the Planck's constant and m^* is the electron effective mass in conduction band. The linear fitting of blueshift (ΔE_g) versus n_e is shown in the inset of Fig. 9. It was found that the optical band gap energy had a linear dependence on the carrier concentration n_e. To determine the relation between ΔE_g and carrier concentration quantitatively, set $m^* = 0.28\ m_0$, where m_0 is the free electron mass and substitute measured values of ΔE_g and n_e into Eq. (2) [53]. The calculated exponent of n_e was 0.657–0.659 with the $H_2/(Ar + H_2)$ ratio of 0–10%, which was close to the theoretical value of 0.667.

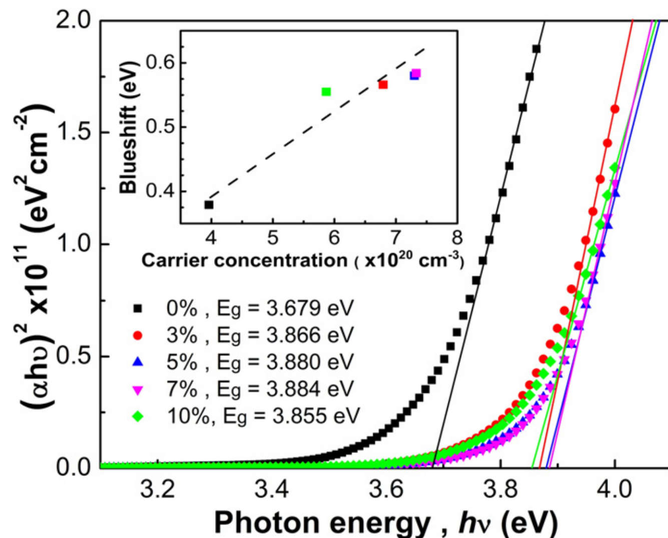

Fig. 9. Plot of $(\alpha h\upsilon)^2$ vs. photon energy of AFZO:H thin films with various $H_2/(H_2 + Ar)$ ratios. The inset shows blue-shift as a function of carrier concentration.

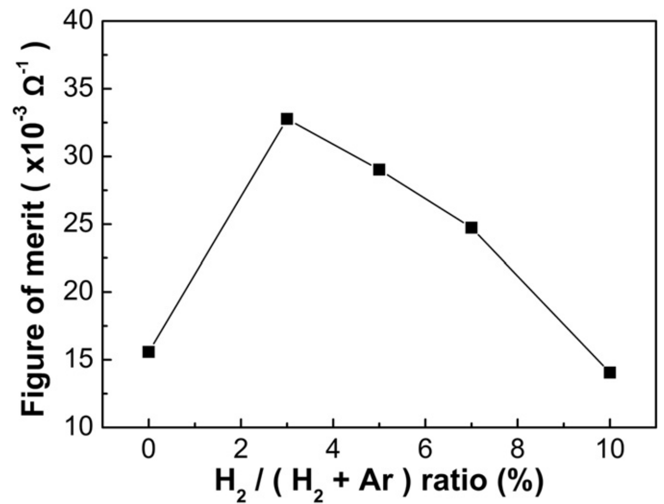

Fig. 10. FOM of AFZO:H thin films with different $H_2/(H_2 + Ar)$ ratios.

The beneficial effect of hydrogen doping can be examined more clearly by calculating the figure of merit (FOM). Haacke defined the quantitative measure for the FOM by T^{10}/R_S [54], where T is the average

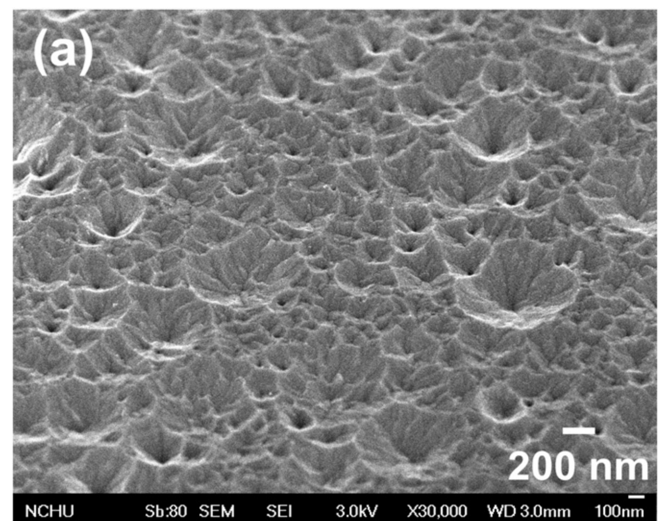

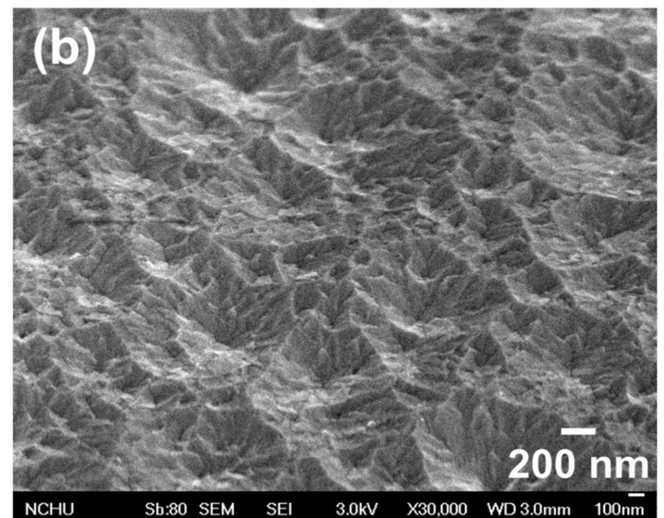

Fig. 11. Surface morphology of 0.2%-HCl etched AFZO films with the $H_2/(H_2 + Ar)$ ratios of (a) 0% and (b) 3%.

optical transmittance and R_S is the sheet resistance of films. Therefore, in order to know the impact of the hydrogen doping on the performance of AFZO films, the FOM values for different $H_2/(Ar + H_2)$ ratios are computed, as Fig. 10 shows. The maximum FOM value was obtained for the films with the $H_2/(Ar + H_2)$ ratio of 3%. Subsequently the optimum AFZO films along with the unhydrogenated one are used as front transparent electrodes for further study on performance of α-Si thin film solar cells.

It is known that the front TCO electrodes with textured surface can scatter incident light at the TCO/α-Si:H interface to increase haze ratio, and thus to extend its effective path length within the active i-layer and subsequent light trapping inside the absorber material of solar cells [55]. In this study, 0.2%-HCl etching of the AFZO films has been executed to develop the textured surfaces. Fig. 11 displays the surface morphology of the etched AFZO thin films with the $H_2/(Ar + H_2)$ ratios

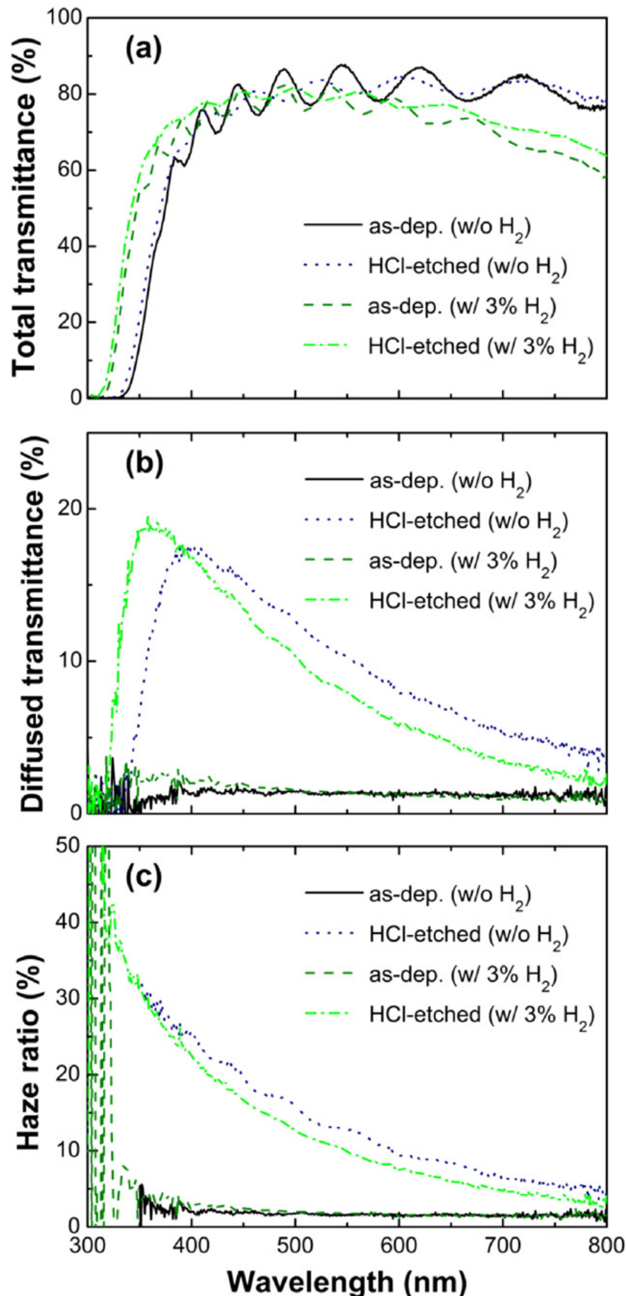

Fig. 12. (a) Total transmittance, (b) diffused transmittance, and (c) haze ratio for the as-deposited and HCl-etched AFZO thin films.

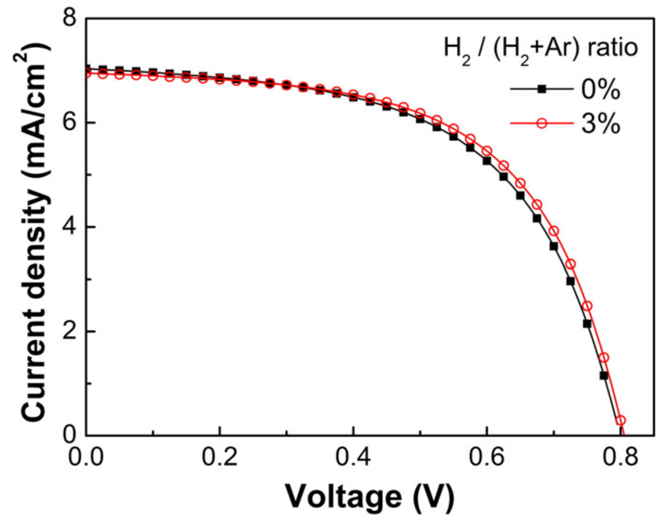

Fig. 13. Current density–voltage characteristics of developed superstrate p-i-n hydrogenated α-Si thin film solar cells under AM 1.5 G illumination.

of 0 and 3%. After HCl etching, the films surfaces formed many crater-like caves and the surface roughness considerably increased. Fig. 12 shows the total, diffused transmittance and haze ratio for the as-deposited and HCl-etched AFZO thin films. The etched AFZO film with hydrogen doping has higher total and diffused transmittance in the short wavelength range (300–400 nm) than that without hydrogen incorporation, while the result was reversed in the medium-long wavelength range (450–800 nm). The haze ratio was determined by diffused transmittance/total transmittance and its average values from 350 to 800 nm increased from 1.75% and 2.02% to 13.3% and 11.2% for the films with the $H_2/(Ar + H_2)$ ratio of 0% and 3%, respectively. The high diffused transmittance and haze ratio reveal effective light-trapping in solar cells with the unhydrogenated AFZO film.

The superstrate p-i-n hydrogenated α-Si thin film solar cells were fabricated at 200 °C using the textured AFZO thin films as front electrodes. No antireflective coatings were deposited on the cells. The subsequent processes of solar cells were carried out in the same batch in order for making a proper comparison between cells with different transparent electrodes. To understand the influence of the deposition temperature of the α-Si film on electrical property of the AFZO films, their resistivities after 200 °C annealing in vacuum for 1 h were measured. The resistivity of the unhydrogenated AFZO films slightly decreased from 0.917 to 0.839 mΩ-cm, while that with 3% H_2 slightly increased from 0.441 to 0.568 mΩ-cm. The changes in the resistivities of the AFZO films after 200 °C-annealing were relatively small. Fig. 13 shows the current density–voltage characteristics of the fabricated solar cells under AM 1.5G illumination. Table 3 lists the values of open-circuit voltage (V_{oc}), short-circuit current density (J_{sc}), fill factor (FF), and energy conversion efficiency (η). The calculated series resistance (R_s) of the cells with 3% hydrogen in the TCO process, 20.4 Ω-cm^2, is lower than that without hydrogen (23.8 Ω-cm^2). This result may be attributed to the lower resistivity for the hydrogenated AFZO film and further leads to higher V_{oc} and FF than that of the unhydrogenated one. However, the decreased J_{sc} in the cell with the hydrogenated AFZO film is due to the lower total transmittance and haze ratio of the film. Hence, the efficiency of the solar cell with the

Table 3
Values of open-circuit voltage (V_{oc}), short-circuit current density (J_{sc}), fill factor (FF), and efficiency (η).

$H_2/(Ar + H_2)$ ratio	V_{oc} (V)	J_{sc} (mA/cm^2)	FF (%)	Efficiency (%)
0%	0.800	7.083	56.39	3.17
3%	0.810	6.953	58.20	3.28

hydrogenated TCO film is only slightly larger (3.5%) than that without hydrogenation.

4. Conclusions

Transparent conducting AFZO:H thin films were deposited, characterized, as well as used as front electrodes of silicon thin film solar cells. All the AFZO thin films exhibit a typical wurtzite structure with a (0 0 2) preferential orientation of the c-axis perpendicular to the substrate. The electrical, optical, and structural properties of the AFZO films prepared with different $H_2/(Ar + H_2)$ ratios varied with the different hydrogen gas ratio in sputtering ambient. The optimal $H_2/(Ar + H_2)$ ratio for preparing low resistant and high transparent AFZO thin films at RT was 3%. The minimum resistivity of the AFZO:H film was as low as 4.41×10^{-4} Ω-cm. The average optical transmittance in the visible wavelength range (400–700 nm) was larger than 92% for all the AFZO films regardless of hydrogen content. Furthermore, the superstrate p-i-n hydrogenated α-Si thin film solar cell with the hydrogenated AFZO thin film as the front electrode has the higher open-circuit voltage, fill factor, and energy conversion efficiency than those without hydrogenation. These results indicate that AFZO:H films are promising as window layers in solar cells.

Acknowledgments

The authors would like to thank the National Science Council of Taiwan under the Grant NSC 102-2221-E-005-068 for the financial support.

References

[1] D.S. Ginley, C. Bright, Transparent conducting oxides, MRS Bull. 25 (2000) 15–18.
[2] H.R. Kim, G.H. Lee, D.H. Kim, Effects of hydrogen plasma treatment on the structural and electrical properties of sputter-deposited SnO_2 thin films, J. Phys. D. Appl. Phys. 44 (2011) 185203.
[3] J. Hüpkes, B. Recha, O. Kluth, T. Repmann, B. Zwaygardt, J. Muller, R. Drese, M. Wuttig, Surface textured MF-sputtered ZnO films for microcrystalline silicon-based thin-film solar cells, Sol. Energy Mater. Sol. Cells 90 (2006) 3054–3060.
[4] T. Minami, Transparent conducting oxide semiconductors for transparent electrodes, Semicond. Sci. Technol. 20 (2005) S35–S44.
[5] T. Tohsophon, J. Hüpkes, H. Siekmann, B. Rech, M. Schultheis, N. Sirikulrat, High rate direct current magnetron sputtered and texture-etched zinc oxide films for silicon thin film solar cells, Thin Solid Films 516 (2008) 4628–4632.
[6] S. Faÿ, J. Steinhauser, S. Nicolay, C. Ballif, Polycrystalline ZnO: B grown by LPCVD as TCO for thin film silicon solar cells, Thin Solid Films 518 (2010) 2961–2966.
[7] J.S. Cho, S. Baek, J.C. Lee, Surface texturing of sputtered ZnO:Al/Ag back reflectors for flexible silicon thin-film solar cells, Sol. Energy Mater. Sol. Cells 95 (2011) 1852–1858.
[8] F.H. Wang, H.P. Chang, C.C. Tseng, C.C. Huang, Effects of H_2 plasma treatment on properties of ZnO:Al thin films prepared by RF magnetron sputtering, Surf. Coat. Technol. 205 (2011) 5269–5277.
[9] J. Nomoto, Y. Nishi, T. Miyata, T. Minami, Influence of the kind and content of doped impurities on impurity-doped ZnO transparent electrode applications in thin-film solar cells, Thin Solid Films 535 (2013) 426–431.
[10] C.C. Huang, F.H. Wang, C.F. Yang, H.H. Huang, Influences of deposition power of GZO thin films on the properties of the heterojunction diode based on a NiO/GZO bi-layer structure, Int. J. Nanotechnol. 11 (2014) 287–297.
[11] F.H. Wang, J.C. Chao, H.W. Liu, T.K. Kang, Physical properties of ZnO thin films co doped with titanium and hydrogen prepared by rf magnetron sputtering with different substrate temperatures, J. Nanomater. (2015), 936482 (11 pages).
[12] Y.C. Lin, T.Y. Chen, L.C. Wang, S.Y. Lien, Comparison of AZO, GZO, and AGZO thin films TCOs applied for a-Si solar cells, J. Electrochem. Soc. 159 (2012) H599–H604.
[13] A.V. Moholkar, S.M. Pawar, K.Y. Rajpure, V. Ganesan, C.H. Bhosale, Effect of precursor concentration on the properties of ITO thin films, J. Alloys Compd. 464 (2008) 387–392.
[14] R.E. Treharne, K. Durose, Fluorine doped ZnO thin films by rf magnetron sputtering, Thin Solid Films 519 (2011) 7579–7582.
[15] F.H. Wang, C.F. Yang, Y.H. Lee, Deposition of F-doped ZnO transparent thin films using ZnF_2-doped ZnO target under different sputtering substrate temperatures, Nanoscale Res. Lett. 9 (2014) 97 7 pages.
[16] R.G. Gordon, Criteria for choosing transparent conductors, MRS Bull. 25 (8) (2000) 52–57.
[17] B.L. Zhu, J. Wang, Thickness study of AZO films by rf sputtering in $Ar + H_2$ atmosphere at room temperature, Phys. Status Solidi A 209 (2012) 1251–1258.
[18] H.B. Zhou, H.Y. Zhang, Effects of substrate temperature on the efficiency of hydrogen incorporation on the properties of Al-doped ZnO films, Superlattice. Microst. 51 (2012) 644–650.
[19] S.J. Tark, Y.W. Ok, M.G. Kang, H.J. Lim, W.M. Kim, D. Kim, Effect of a hydrogen ratio in electrical and optical properties of hydrogenated Al-doped ZnO films, J. Electroceram. 23 (2009) 548–553.
[20] Z. Pan, Y. Xiao, X. Tian, S. Wu, C. Chen, J. Deng, C. Xiao, G. Hu, Z. Wei, Effect of annealing on the structures and properties of Al and F co-doped ZnO nanostructures, Mater. Sci. Semicond. Process. 17 (2014) 162–167.
[21] A. Maldonado, S. Tirado-Guerra, J.M. Cázares, M.d.l.L. Olvera, Physical and sensing properties of ZnO:F:Al thin films deposited by sol–gel, Thin Solid Films 518 (2010) 1815–1820.
[22] D.C. Altamirano-Juárez, G. Torres-Delgado, S. Jimenez-Sandoval, O. Jimenez-Sandoval, R. Castanedo-Perez, Low-resistivity ZnO:F:Al transparent thin films, Sol. Energy Mater. Sol. Cells 82 (2004) 35–43.
[23] B. Zhou, X. Han, M. Tao, Al and F codoped ZnO by a novel co-spray deposition technique for solar cells applications, Tampa, Florida, U.S.A., June 16–21, 2013, IEEE Photovoltaic Specialists Conference 2013, pp. 1195–1198.
[24] Y.H. Kim, J. Jeong, K.S. Lee, J.K. Park, Y.J. Baik, T.Y. Seong, W.M. Kim, Characteristics of ZnO:Al thin films co-doped with hydrogen and fluorine, Appl. Surf. Sci. 256 (2010) 5102–5107.
[25] I. Kim, K.S. Lee, T.S. Lee, J.H. Jeong, B.K. Cheong, Y.J. Baik, W.M. Kim, Effect of fluorine addition on transparent and conducting Al doped ZnO films, J. Appl. Phys. 100 (2006) 063701.
[26] B. Houng, H.B. Chen, Effect of discharge power density on the properties of Al and F co-doped ZnO thin films prepared at room temperature, J. Electroceram. 29 (2012) 1–7.
[27] F.H. Wang, S.C. Hung, C.F. Yang, Y.H. Lee, Effects of hydrogen plasma on the electrical properties of F-doped ZnO thin films and p-i-n α-Si:H thin film solar cells, Int. J. Photoenergy (2014), 425057 (7 pages).
[28] S.H. Lee, T.S. Lee, K.S. Lee, B. Cheong, Y.D. Kim, W.M. Kim, Characteristics of hydrogen co-doped ZnO:Al thin films, J. Phys. D. Appl. Phys. 41 (2008) 095303.
[29] W. Liu, G. Du, Y. Sun, Y. Xu, T. Yang, X. Wang, Y. Chang, F. Qiu, Al-doped ZnO thin films deposited by reactive frequency magnetron sputtering: H_2-induced property changes, Thin Solid Films 515 (2007) 3057–3060.
[30] B.D. Cullity, S.R. Stock, Elements of XRD, Prentice Hall, 2001 167–171 (Chap. 5-2).
[31] X.Y. Lia, H.J. Lia, Z.J. Wang, H. Xia, Z.Y. Xiong, J.X. Wang, B.C. Yang, Effect of substrate temperature on the structural and optical properties of ZnO and Al-doped ZnO thin films prepared by dc magnetron sputtering, Opt. Commun. 282 (2009) 247–252.
[32] C.C. Huang, F.H. Wang, C.F. Yang, Effects of deposition temperature and hydrogen flow rate on the properties of the Al-doped ZnO thin films and amorphous silicon thin-film solar cells, Appl. Phys. A Mater. Sci. Process. 112 (2013) 877–883.
[33] D. Raoufi, T. Raoufi, The effect of heat treatment on the physical properties of sol–gel derived ZnO thin films, Appl. Surf. Sci. 255 (2009) 5812–5817.
[34] W.F. Liu, G.T. Du, Effects of hydrogen flux on the properties of Al-doped ZnO films sputtered in $Ar + H_2$ ambient at low temperature, Appl. Surf. Sci. 253 (2007) 2999–3003.
[35] M.L. Addonizio, A. Antonaia, G. Cantele, C. Privato, Transport mechanisms of RF sputtered Al-doped ZnO films by H_2 process gas dilution, Thin Solid Films 349 (1999) 93–99.
[36] J.H. Lee, Effects of hydrogen incorporation and heat treatment on the properties of ZnO:Al films deposited on polymer substrate for flexible solar cell applications, Curr. Appl. Phys. 10 (2010) S515–S519.
[37] Y. Hu, Y. Chen, J. Chen, X. Chen, D. Ma, Effects of hydrogen flow on properties of hydrogen doped ZnO thin films prepared by RF magnetron sputtering, Appl. Phys. A Mater. Sci. Process. 114 (2014) 875–882.
[38] Y.R. PARK, D. Jung, Y.S. Kim, Organic solar cells with hydrogenated In-doped ZnO replacing Sn-doped In_2O_3 as transparent electrode, Jpn. J. Appl. Phys. 47 (2008) 516–520.
[39] C.G. Van de walle, J. Neugebauer, Universal alignment of hydrogen levels in semiconductors, insulators and solutions, Nature 423 (2003) 626.
[40] J.N. Duenow, T.A. Gessert, Effects of hydrogen content in sputtering ambient on ZnO:Al electrical properties, J. Non-Cryst. Solids 354 (2008) 2787–2790.
[41] M.N. Islam, T.B. Ghosh, K.L. Chopra, H.N. Acharya, XPS and X-ray diffraction studies of aluminum-doped zinc oxide transparent conducting films, Thin Solid Films 280 (1996) 20–25.
[42] M. Chen, X. Wang, Y.H. Yu, Z.L. Pei, X.D. Bai, C. Sun, R.F. Huang, L.S. Wen, X-ray photoelectron spectroscopy and auger electron spectroscopy studies of Al-doped ZnO films, Appl. Surf. Sci. 158 (2000) 134–140.
[43] J.P. Kar, S. Kim, B. Shin, K.I. Park, K.J. Ahn, W. Lee, J.H. Cho, J.M. Myoung, Influence of sputtering pressure on morphological, mechanical and electrical properties of Al-doped ZnO films, Solid State Electron. 54 (2010) 1447–1450.
[44] K. Uma, M. Rusop, T. Soga, T. Jimbo, Effects of Al content on $Zn_{0.95}Mg_{0.05}O$ thin films deposited by sol–gel spin coating, Jpn. J. Appl. Phys. 46 (2007) 40–44.
[45] H.P. Chang, F.H. Wang, J.Y. Wu, C.Y. Kung, H.W. Liu, Enhanced conductivity of aluminum doped ZnO films by hydrogen plasma treatment, Thin Solid Films 518 (2010) 7445–7449.
[46] C.G. Van de Walle, Hydrogen as a cause of doping in zinc oxide, Phys. Rev. Lett. 85 (2000) 1012–1015.
[47] J. Cho, K.H. Yoon, M.S. Oh, W.K. Choi, Effects of H_2 annealing treatment on photoluminescence and structure of $ZnO:Al/Al_2O_3$ grown by radio-frequency magnetron sputtering, J. Electrochem. Soc. 150 (2003) H225–H228.
[48] H.L. Hartnagel, A.L. Dawar, A.K. Jain, C. Jagadish, Semiconducting Transparent Thin Films, Institute of Physics Publishing, Philadelphia, 1995.
[49] J.F. Chang, M.H. Hon, The effect of deposition temperature on the properties of Al-doped zinc oxide thin films, Thin Solid Films 386 (2001) 79–86.
[50] E. Burstein, Anomalous optical absorption limit in InSb, Phys. Rev. 93 (1954) 632–633.

[51] B. Houng, H.B. Chen, Investigation of $A1F_3$ doped ZnO thin films prepared by RF magnetron sputtering, Ceram. Int. 38 (2012) 801–809.
[52] T.S. Moss, The interpretation of the properties of indium antimonide, Proc. Phys. Soc. B 67 (1964) 775–782.
[53] B.E. Sernelius, K.F. Berggren, Z.C. Jin, I. Hamberg, C.G. Granqvist, Band-gap tailoring of ZnO by means of heavy Al doping, Phys. Rev. B 37 (1988) 10244–10248.
[54] G. Haacke, New figure of merit for transparent conductors, J. Appl. Phys. 47 (1976) 4086–4089.
[55] F. Wang, H. Chang, C. Tseng, C. Huang, H. Liu, Influence of hydrogen plasma treatment on Al-doped ZnO thin films for amorphous silicon thin film solar cells, Curr. Appl. Phys. 11 (2011) S12–S16.